LAWRENCE
LIVERMORE
NATIONAL
LABORATORY

UCRL-JC-152388

Electronic Structure Measurement of Solid Density Plasmas using X-Ray Scattering

G. Gregori, S. H. Glenzer, F. J. Rogers, O. L. Landen, C. Blancard, G. Faussurier, P. Renaudin, S. Kuhlbrodt, R. Redmer

August 23, 2003

2003 Third International Conference on Inertial Fusion Sciences and Applications, Monterey, CA
September 7-12, 2003

Electronic structure measurement of solid density plasmas using x-ray scattering

G. Gregori*, S. H. Glenzer*, F. J. Rogers*, O. L. Landen*, C. Blancard†, G. Faussurier†, P. Renaudin†, S. Kuhlbrodt** and R. Redmer**

*Lawrence Livermore National Laboratory, PO Box 5508, Livermore, CA 94551
†Département de Physique Théorique et Appliquée, CEA/DAM Ile-de-France, BP12, 91680 Bruyéres-le-Châtel Cedex, France
**Universität Rostock, Fachbereich Physik, Universitätsplatz, 3, D-18051, Rostock, Germany

Abstract. We present an improved analytical expression for the x-ray dynamic structure factor from a dense plasma which includes the effects of weakly bound electrons. This result can be applied to describe scattering from low to moderate Z plasmas, and it covers the entire range of plasma conditions that can be found in inertial confinement fusion experiments, from ideal to degenerate up to moderately coupled systems. We use our theory to interpret x-ray scattering experiments from solid density carbon plasma and to extract accurate measurements of electron temperature, electron density and charge state. We use our experimental results to validate various equation-of-state models for carbon plasmas.

1. INTRODUCTION

X-ray scattering of solid density plasmas has recently been proven a successful technique for the characterization of low-Z warm and dense states of matter [1, 2, 3]. In particular, it was shown that by extending the theory of spectrally resolved Thomson scattering to the hard x-ray regime, accurate measurements of the electron temperature, electron density and ionization state can be obtained. In this respect, comparison of the experimental results with equation of state (EOS) models has started revealing important insights on the microscopic electronic state of solid density beryllium plasmas [1]. In this paper, we present a generalization of the technique to higher Z materials, thus allowing the study of basic plasma parameters and transport properties of a vast range of plasma regimes, as the ones created in high energy density experiments relevant for inertial confinement fusion (ICF) [4] and found in the interior of stars and planets.

In the case of low-Z materials, the x-ray dynamic form factor, which is the fundamental quantity describing the scattering cross section, is considerably simplified since it contains only two major contributions that arise from scattering from free electrons and tightly bound electrons. The first term is usually described within the random phase approximation (RPA) [5, 6] and it refers to photon scattering from density fluctuations of the free electrons in the plasma. During the process, energy is exchanged from the photons to the electrons, and the scattered photons are downshifted in energy by the Compton effect. Elastic scattering from tightly bound electrons, instead, arises from photons that elastically scatter electrons, as energy transfer is not kinematically allowed. In this case, electrons cannot be excited from deep states into the continuum. The x-ray scattering cross section can be thus obtained for solid density matter, accounting for both ideal and quantum degenerate plasmas [3]. The transition from ideal to degenerate states often encompasses weakly or strongly coupled states [7] which may exhibit a modified response in the electron density fluctuation dynamics. A discussion on such conditions and their effect on the x-ray scattering form factor has been presented previously [8].

X-ray scattering from moderate to high-Z materials add another term to the total form factor: scattering from weakly bound electrons. Since, for those electrons Compton scattering is kinematically permitted, the incident x-ray photons have a certain probability to transfer a portion of their energy and momentum to the electrons, resulting in the appearance of a secondary inelastic scattering feature in the spectrum of the scattered radiation that overlaps with the free electron one. Thus, the interplay of the scattering from all of these terms: free, tightly bound and weakly bound electrons, provides a unique method for a full characterization of the electronic state of the dense plasma. The number of valence (or delocalized) electrons can be directly inferred from the experimental spectra for the experimental conditions of this work, as well as electron temperature and density, pro-

viding important EOS model validation. We will further discuss this point using carbon as an example. By extracting carbon EOS data from experimental x-ray scattering spectra from solid density carbon plasmas, we can directly test various ionization balance models of solid density plasmas.

2. THEORY

Following the discussion in Ref. [3], we describe the scattering from a uniform plasma containing N ions per unit volume. If Z_A is the nuclear charge of the ion, the total number of electrons per unit volume in the system, including free and bound ones, is $Z_A N$. Let us now assume we probe such a system with x-rays of frequency ω_0 such that $\hbar\omega_0 \gg E_I$, with E_I the ionization energy of any bound electron, *i.e.*, the incident frequency must be large compared to any natural absorption frequency of the scattering atom, which allows us to neglect resonant scattering. During the scattering process, the incident photon transfers momentum $\hbar\mathbf{k}$ and energy $\hbar\omega = \hbar\omega_0 - \hbar\omega_1$ to the electron, where ω_1 is the frequency of the scattered radiation, and in the non-relativistic limit ($\hbar\omega \ll \hbar\omega_0$) $k = |\mathbf{k}| = \frac{4\pi}{\lambda_0}\sin(\theta/2)$, with λ_0 the probe wavelength and θ the scattering angle. We denote with Z_f and Z_c the number of kinematically free and bound electrons, respectively. Clearly, $Z_A = Z_f + Z_c$. Here Z_c includes both tightly bound and weakly bound electrons, as there is not a net distinction between them, and for any given bound electron in the outermost shells there is a finite probability of either elastic or inelastic scattering. Since Z_f represents electrons which are not bound to any single atom, we will also refer to it as the number of delocalized, or valence, electrons. Following the approach of Chihara [9, 10] the scattering cross section is described in terms of the dynamic structure factor of all the electrons in the plasma:

$$S(k,\omega) = |f_I(k) + q(k)|^2 S_{ii}(k,\omega) + Z_f S^0_{ee}(k,\omega) + Z_c \int \tilde{S}_{ce}(k,\omega-\omega') S_s(k,\omega') d\omega'. \quad (1)$$

The first term in Eq. (1) accounts for the density correlations of electrons that dynamically follow the ion motion. This includes both the bound electrons, represented by the ion form factor $f_I(k)$, and the screening cloud of free (and valence) electrons that surround the ion, represented by $q(k)$ [11]. $S_{ii}(k,\omega)$ is the ion-ion density correlation function. The second term in Eq. (1) gives the contribution in the scattering from the free electrons that do not follow the ion motion. Here, $S^0_{ee}(k,\omega)$ is the high frequency part of the electron-electron correlation function [12] and it reduces to the usual electron feature [13, 14] in the case of an optical probe. Inelastic scattering by bound electrons is included in the last term of Eq. (1), which arises from bound-free transitions to the continuum of core electrons within an ion, $\tilde{S}_{ce}(k,\omega)$, modulated by the self-motion of the ions, represented by $S_s(k,\omega)$.

In Ref. [3], we have presented simplified expressions for each term in Eq. (1) for low-Z materials. In those cases, the bound-free contribution is small under most experimental conditions and it can be neglected. However, in the case of carbon, L-shell inelastic scattering needs to be included. Differently from the approach followed in Ref. [3], we propose a more comprehensive treatment of the core electron term based on the impulse approximation (IA) [15, 16]. The IA assumes that the electron-photon interaction occurs on a very short timescale, so the target electron always sees the same nuclear potential just before and after the collision. Since only changes in the kinetic energy needs to be considered, the electron can be treated as free and its final energy depends on the projection of the electron's initial momentum on the scattering vector $\mathbf{k}$. Thus, the Doppler broadening of the scattered radiation is proportional to the initial momentum distribution of the electron [17]. In the hydrogenic approximation for the initial wavefunction and momentum distribution of the electron, the IA profiles for K and L-shells assume the form [18]

$$J_{1,0}(\xi) = \frac{8}{3\pi Z_*(1+\xi^2/Z_*^2)^3}, \quad (2)$$

$$J_{2,0}(\xi) = \frac{64}{\pi Z_*}\left[\frac{1}{3(1+4\xi^2/Z_*^2)^3} - \frac{1}{(1+4\xi^2/Z_*^2)^4} + \frac{4}{5(1+4\xi^2/Z_*^2)^5}\right], \quad (3)$$

$$J_{2,1}(\xi) = \frac{64}{15\pi Z_*}\frac{1+20\xi^2/Z_*^2}{(1+4\xi^2/Z_*^2)^5}, \quad (4)$$

where,

$$\xi = \frac{m_e a_B}{\hbar k}\left(\omega - \frac{\hbar k^2}{2m_e}\right), \quad (5)$$

with a_B the Bohr radius and $Z_* = Z_A - z_{n,l}$ the effective nuclear charge seen by the electron in the quantum state n,l. The screening constants $z_{n,l}$ depend on the atomic (or ionic) state of the atom and they can be calculated from the prescription of Pauling and Sherman [19].

As discussed by Eisenberger and Platzman [15], the IA is correct to the order of $(E_B/E_c)^2$, where E_B is the binding energy and $E_c = \hbar^2 k^2/2m_e$ is the Compton recoil. For our typical experimental conditions, $E_c \sim 70$ eV and the binding energy of L-shell carbon electrons is $E_B \sim 11$-64 eV (depending on the ionization state), thus errors introduced by the IA can be significant. Even if K-shell contribution is typically less important than the L-shell one, corrections to the IA need to be accounted

for K-shell electrons as well. The main modification in the IA appears as a shift of the peak of feature from the free electron value, an effect known as the Compton defect [20, 21]. Since the IA assumes plane waves as the final state for the electron, improvement in the model can be obtained by using the first Born approximation and hydrogenic wavefunctions for both initial and final states [15, 22, 23], or by a perturbation expansion of the final states [24, 25]. In our work we will follow the perturbative approach of Holm and Ribberfors [25]. The total bound-free dynamic structure is thus written as

$$\tilde{S}_{ce}(k,\omega) = \frac{r_k}{Z_c} \sum_{n,l} J_{n,l}(\xi), \qquad (6)$$

with the sum running over all the bound electrons. The normalization constant r_k accounts for the possibility of coherent scattering [26].

Profiles of the bound-free dynamic structure for a carbon plasma are given in Figure 1a for different ionization states and typical experimental conditions. The carbon is assumed to be in an amorphous state (foam) with density 0.72 g/cc. In the high frequency limit, the ion-ion self structure is $S_s(k,\omega) \sim \delta(\omega)$, as ion dynamics remain unresolved under our experimental conditions [3]. Since bound-free transitions are not allowed if $\hbar\omega < E_B$, the dynamic factor (6) has a cut-off at the ionization energy for L-shell electrons, as it is clearly shown in Figure 1a. Similarly, for K-shell electrons, the cut-off marks the K-shell binding energy.

In the case of very dense plasmas, the electric field distribution of a given ion is influenced not only by its own bound electrons but also by the neighboring ions. The net effect is a lowering of the ionization potential (*continuum lowering*). Such lowering depends on the total number of ions that participate in the modification of the potential around a test ion, which, in turn, is a function of the screening distance of the Coulomb forces. Stewart and Pyatt [27] have calculated the continuum lowering (ΔE_B) using a finite-temperature Thomas-Fermi model which reproduces both the classical Debye screening for low density plasmas and the ion-sphere correlation length for high density coupled systems. For typical experimental conditions, ΔE_B accounts for ~30-50% of the ionization energy, thus continuum lowering strongly shifts the L-shell edges of the bound-free dynamic structure.

3. EXPERIMENTAL RESULTS

We apply the calculation technique discussed in the previous section to a dense carbon plasma. We used the 30-kJ Omega laser facility [28] to produce a homogeneous and isochorically heated carbon plasma at solid density, and then probed the plasma interior with the Ti He-α x-ray line at 4.75 keV from a secondary laser produced plasma. The details of the experimental technique have been extensively discussed in Refs. [1, 2]. Prior to laser heating, the carbon is in an amorphous (foam) state with density 0.72 g/cc. Since during the heating and probing times the plasma is not globally expanding (see Ref. [2]), the initial carbon density sets the ion density to $n_i = 3.6 \times 10^{22}$ cm^{-3}. The electron density is then determined by the ionization state of the system. By changing the number of heating beams, we can vary the degree of carbon heating and consequently its ionization state.

In Figure 1b we have plotted experimental profiles obtained for two different cases: a strongly heated foam and a cold one. The scattered radiation has been collected at a scattering angle of $\sim 130^\circ \pm 5^\circ$ with a high efficiency graphite Bragg crystal operated in mosaic focusing mode [1, 2]. This geometry corresponds to a scattering parameter $\alpha = 1/k\lambda_{De} < 1$, where $\lambda_{De} = \sqrt{\varepsilon_0 k_B T_{cf}/n_e e^2}$, and T_{cf} is a modified electron temperature that mimic quantum degeneracy [3]. Thus the scattering is noncollective and the inelastic scattering spectra of the free electrons directly show the distribution function. From the figure we notice an increased red wing for the higher temperature foam, indicating that a larger number of electrons have been downshifted in energy by the Compton effect. Since these are essentially free electrons, an increased red wing in the spectrum is thus a signature of a higher ionization state. By combining the theory outlined in the previous section for the core electrons with the approach based on the RPA for the free electron density response [3], we can fit the experimental data to obtain T_e and Z_f. The electron density is then simply given as $n_e = Z_f n_i$, as heating is isochoric and the plasma does not expand at the probing time. The high temperature foam gives $Z_f = 4.25$ and $T_e = 52$ eV, while for the cold foam $Z_f = 0.26$ and $T_e = 5$ eV. The error in the temperature measurement for the high temperature foam has been determined to be $\lesssim$20% [1]. For the cold foam, instead, the electron plasma is fully degenerate ($T_e \sim T_F$) and the width of the Compton feature is only weakly sensitive on the electron temperature. Moreover, the Compton profile mainly results from bound-free transitions which directly reflects the ion temperature. Under these conditions, the fitted temperature is understood only as an upper limit of the actual electron temperature of the degenerate electron fluid. As a final remark, we notice that for our experimental conditions, the electron-electron coupling constant $\Gamma = e^2/4\pi\varepsilon_0 k_B T_{cf} d \lesssim 1$, thus local field corrections to the RPA are not important [8].

Figure 2 shows the T_e-Z_f phase diagram along with experimental data and various EOS models for carbon. These are the activity expansion method (ACTEX) [29, 30], the partially ionized plasma (PIP) model [31, 32] and SCAALP, a density functional plasma model [33].

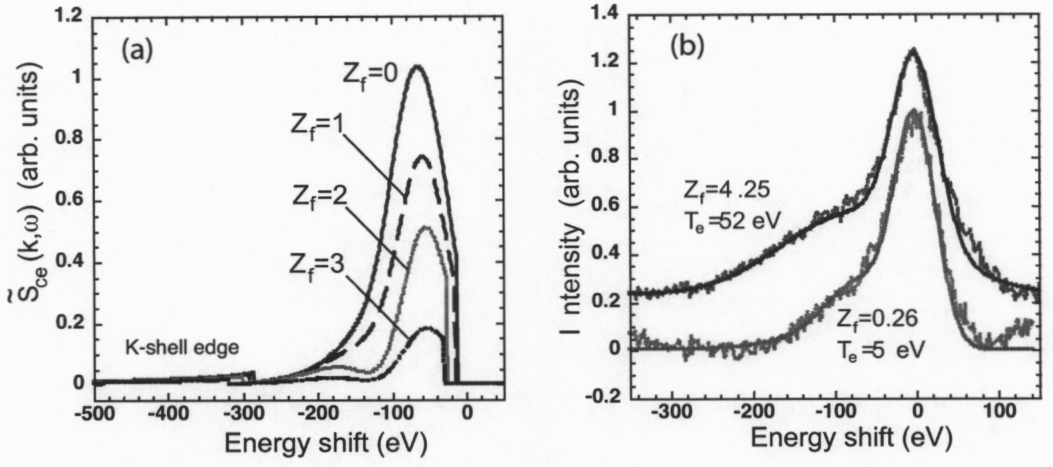

FIGURE 1. (a) Calculated bound-free dynamic structures, $\tilde{S}_{ce}(k,\omega)$, for a carbon plasma with density 0.72 g/cc at 130° scattering angle. The probe energy is $E_0 = 4.75$ keV. The ionization energy is corrected for continuum lowering. (b) Experimental x-ray scattering data from a heated carbon foam (0.72 g/cc) and a cold carbon foam. The probe radiation is the Ti He-α line at 4.75 keV, and the scattered x-rays are collected at $\sim 130^{\circ} \pm 5^{\circ}$ scattering angle. Best fit parameters and corresponding spectra are also plotted in the figure. For the high temperature foam, $\alpha = 0.17$, $T_F = 10.4$ eV, and $\Gamma = 0.2$; while for the cold foam $\alpha = 0.13$, $T_F = 1.6$ eV, and $\Gamma = 0.9$.

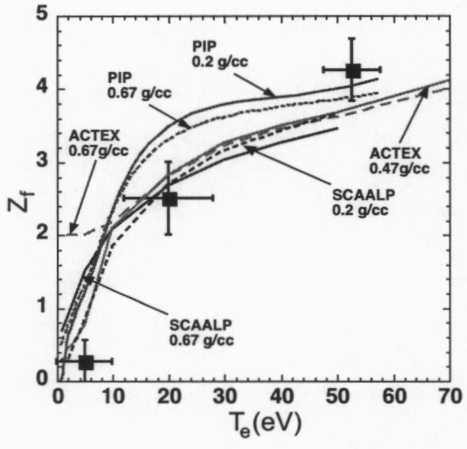

FIGURE 2. Temperature-ionization diagram along with the results of the x-ray scattering measurements and various EOS models (see text).

In the ACTEX theory, all possible interactions between plasma constituents are calculated including the screening of the bound states. For large densities, the classical Debye-Hückel (Yukawa) potential is replaced by a screened potential which has a cut-off for distances that approach the thermal de Broglie wavelength, in order to mimic quantum mechanical effects (*i.e.,* exchange and symmetry). This approach allows the calculation of delocalized electrons, i.e., the number of electrons that are no longer bound to a single ion. These electrons are free or weakly bound like the conduction electrons in a metal. For our conditions, these electrons give rise to the Compton downshifted electron feature of the x-ray scattering spectrum. The PIP model is based on the self-consistent solution of Saha-like equations for each ionization stage together with the calculation of appropriate chemical potentials for electrons and ions. This also allows the inclusion of high density effects by using corrected chemical potentials for the continuum lowering. SCAALP is based on the density functional theory for plasmas, where electronic structure and ionic distribution are determined self-consistently. The plasma is considered as an effective classical system of virtual neutral particles (neutral pseudo-atom, NPA) interacting via an interatomic effective potential $V_{eff}(r)$. Electrons of the NPA satisfy a Schrodinger equation with an effective central symmetric potential $\phi(r)$. Both V_{eff} and ϕ are determined by the electronic structure and the ionic distribution of the plasma. Polarization and correlation effect of the continuum electrons are taken into account, as well as a part of the exchange interaction within V_{eff}.

Results from these models, assuming several values for the carbon density, are plotted in Figure 2. The comparison with the experimental data shows good agreement with SCAALP at all densities, even if some differences still remain especially for the high temperature case. The PIP model also gives reasonably good agreement with the data at all densities, but it seems to over-predict the ionization state in the mid-temperature regime. In this regime the plasma undergoes a transition from a degenerate fluid to a classical one, thus a full quantum mechanical treatment beyond the Saha de-

scription may be required. ACTEX shows a similar trend to SCAALP for the low density simulation, but, in the higher density case, predicts a low temperature foam which still have ~2 electrons in the conduction band. This transition to a metallic state for carbon at high density are not reproduced by the other models at this density. Our experimental data at low T_e show an insulating behavior for carbon at high density.

From this discussion, we see that currently available EOS models for carbon exhibit different behavior in the temperature range 0-50 eV, which span the range from fully degenerate to classical plasmas. X-ray scattering thus provides an accurate experimental tool for validation and improvement of EOS codes, as shown in Figure 2.

4. CONCLUSIONS

We have provided expressions to calculate the x-ray scattering form factor from weakly bound electrons which are accurate for medium to low-Z materials. The approach that we have followed is based on the IA corrected for the asymmetry induced by the electron binding. Together with the RPA for the free electron dynamic structure, we were able to obtain a full description of the x-ray scattering form factor for a carbon plasma. We have compared our model with experimental data from the Omega laser facility in order to extract accurate values for electron temperature and ionization state. This has allowed the comparison between various ionization balance models for carbon with our data, thus enabling a direct validation of EOS theories for a carbon plasma in a regime which cover the transition between a degenerate to classical fluid. Our result are of interest for ICF research as well as planetary science since they indicate that matter under extreme conditions can be investigated with good accuracy.

ACKNOWLEDGMENTS

This work was performed under the auspices of the U.S. Department of Energy by the University of California Lawrence Livermore National Laboratory under Contract No. W-7405-ENG-48. We also acknowledge support from Laboratory Directed Research and Development grant No. 02-ERD-13.

REFERENCES

1. Glenzer, S. H., Gregori, G., Lee, R. W., Rogers, F. J., Pollaine, S. W., and Landen, O. L., *Phys. Rev. Lett.*, **90**, 175002 (2003).
2. Glenzer, S. H., Gregori, G., Rogers, F. J., Froula, D. H., Pollaine, S. W., Wallace, R. S., and Landen, O. L., *Phys. Plasmas*, **10**, 2433 (2003).
3. Gregori, G., Glenzer, S. H., Rozmus, W., Lee, R. W., and Landen, O. L., *Phys. Rev. E*, **67**, 026412 (2003).
4. Lindl, J. D., *Inertial Confinement Fusion*, Springer-Verlag, New York, 1998.
5. Pines, D., and Bohm, D., *Phys. Rev.*, **85**, 338 (1952).
6. Pines, D., and Nozieres, P., *The Theory of Quantum Fluids*, Addison-Wesley, Redwood, CA, 1990.
7. Ichimaru, S., *Rev. Mod. Phys.*, **54**, 1017 (1982).
8. Gregori, G., Glenzer, S. H., and Landen, O. L., *J. Phys. A: Math Gen.*, **36**, 5971 (2003).
9. Chihara, J., *J. Phys. F: Met. Phys.*, **17**, 295 (1987).
10. Chihara, J., *J. Phys.: Condens. Matter*, **12**, 231 (2000).
11. Riley, D., Woolsey, N. C., McSherry, D., Weaver, I., Djaoui, A., and Nardi, E., *Phys. Rev. Lett.*, **84**, 1704 (2000).
12. Ichimaru, S., *Basic Principles of Plasma Physics*, Addison, Reading, MA, 1973.
13. Salpeter, E. E., *Phys. Rev.*, **120**, 1528 (1960).
14. Evans, D. E., and Katzenstein, J., *Rep. Prog. Phys.*, **32**, 207 (1969).
15. Eisenberger, P., and Platzman, P. M., *Phys. Rev. A*, **2**, 415 (1970).
16. Currat, R., DeCicco, P. D., and Kaplow, R., *Phys. Rev. B*, **3**, 243 (1971).
17. DuMond, J. W. M., *Phys. Rev.*, **29**, 643 (1929).
18. Bloch, B. J., and Mendelsohn, L. B., *Phys. Rev. A*, **12**, 1197 (1975).
19. Pauling, L., and Sherman, J., *Zeit. f. Krist.*, **1**, 81 (1932).
20. Bergstrom, P. M., and Pratt, R. H., *Radiat. Phys. Chem.*, **50**, 3 (1997).
21. Issolah, A., Levy, B., Beswick, A., and Loupias, G., *Phys. Rev. A*, **38**, 4509 (1988).
22. Bloch, B. J., and Mendelsohn, L. B., *Phys. Rev. A*, **9**, 129 (1974).
23. Bell, F., *J. Chem. Phys.*, **85**, 303 (1986).
24. Gasser, F., and Tavard, C., *Phys. Rev. A*, **27**, 117 (1983).
25. Holm, P., and Ribberfors, R., *Phys. Rev. A*, **40**, 6251 (1989).
26. Paakkari, T., and Suortti, P., *Phys. Rev. B*, **9**, 1756 (1974).
27. Stewart, J. C., and Pyatt, K. D., *ApJ*, **1203**, 144 (1966).
28. Soures *et al.*, J. M., *Fusion Technol.*, **30**, 492 (1996).
29. Rogers, F. J., and Young, D. A., *Phys. Rev. E*, **56**, 5876 (1997).
30. Rogers, F. J., *Phys. Plasmas*, **7**, 51 (2000).
31. Redmer, R., *Phys. Rev. E*, **59**, 1073 (1999).
32. Kuhlbrodt, S., and Redmer, R., *Phys. Rev. E*, **62**, 7191 (2000).
33. Renaudin, P., Blancard, C., Faussurier, G., and Noiret, P., *Phys. Rev. Lett.*, **88**, 215001 (2002).